

Contents lists available at ScienceDirect

Physica B: Condensed Matter

journal homepage: www.elsevier.com/locate/physb





Atomic structure and properties of entropy stabilized CuBiI₄

Blair R. Tuttle a,*, John R. Bickel a, Zach J. Willard , Victor T. Barone b, Sanjay V. Khare b

- ^a Department of Physics, Penn State Behrend, Erie, 16563, PA, USA
- b Department of Physics, University of Toledo, Toledo, 43606, OH, USA

ABSTRACT

High quality crystals of $CuBiI_4$ have recently been grown and implemented in optoelectronic devices including solar cells. To clarify the atomic structure of $CuBiI_4$ crystals, we explore the unit cells of these crystals which have site disorder leading to over 10^{13} possible atomic configurations. We employ density-functional-fitted cluster-energy expansion calculations to determine low energy, physically relevant atomic configurations. We also calculate the fundamental properties of the bulk material using these newly discovered configurations. Our results for mechanical and electronic properties are compared with previous work. Configurational entropy is important for $CuBiI_4$ stabilization. The models constructed here will be useful to investigate the atomic level structure-property relations in $CuBiI_4$ – including the role of point defects.

1. Introduction

Ternary metal halide semiconductors are a new promising class of materials under development for various applications including flexible electronics, optoelectronics, and radiation/chemical detectors [1–6]. While silver iodo-bismuthates $(Ag_xBi_yI_{x+3y})$ have been examined extensively over the past decade [6–10], copper iodo-bismuthates have more recently been attracting interest, mainly for opto-electronics but also for thermo-electrics [11]. In particular, $CuBiI_4$ shows promise as a UV absorber for indoor photovoltaics, an application area of growing interest due to the rising Internet of Things [12,13].

Recent experimental investigations have focused on the opto-electronic properties of $CuBiI_4$ for photovoltaic applications. Several independent research groups have been able to grow thin films using a variety of methods. From the analysis of photoluminescence measurements the experimental band gap of $CuBiI_4$ is $\approx 1.8~eV~(1.79~eV~[11], 1.8~eV~[14], 1.81~eV~[15], and 1.84~eV~[16])$. Several thin film solar cells were constructed and photo-conversion efficiencies were found to be $\approx 1~\%~(0.83~\%~[17], 1.10~\%~[14],$ and 1.12~%~[15]), while the maximum possible efficiencies are predicted to be close to 20 % with carrier lifetimes of milli-seconds [16]. For $CuBiI_4$ materials to reach their full application potential, it is desirable to develop an understanding of the relationships between atomic structure and the opto-electronic and other properties.

Unfortunately, the atomic placement of atoms in the $CuBiI_4$ crystalline unit cell has not been established. Recently, new potentially viable $CuBiI_4$ unit cells with 12 atoms have been proposed and these crystals have tri- and/or mono-clinic symmetry [18]. In contrast, recent experimental samples of CuBiI₄ have cubic Fd3m symmetry [11,14-16] with 48 atom unit cells, as established by the early X-ray diffraction results published in 1991 [19]. None of the previously proposed CuBil₄ unit cell models are consistent with the experimentally determined structure. Experimentally, CuBiI₄ has mixed covalent-ionic bonding with stacked layers of BiI6 octahedra and CuI4 tetrahedra. Interestingly, Fourcroy et al. [19] found that CuBiI4 is a site-disordered crystal, meaning that the unit cell has definite lattice sites as in a traditional crystal but, unlike a traditional crystal, the sites are not occupied by one specific atom but instead some sites are occupied by one of two possibilities. The CuBiI4 crystal has three sublattices: one sub-lattice has sites that are evenly shared between Bi and vacancies and another sub-lattice has sites that are shared between Cu and vacancies. The third sub-lattice has only iodine atoms. Because of the site-occupancy disorder, the total number of possible atomic configurations for any one unit cell is more than 1013 [20]. Identifying the experimentally important configurations is an important achievement of this study which employs a new method for examining site-occupancy disorder.

Several theoretical methods have been developed to construct models of site disordered crystals. The virtual crystal approximation is inapplicable in the case of *CuBiI*₄ because of the significantly differing electronic configurations between sites occupied with copper or bismuth versus vacancies [21]. The special quasi-random structure (SQS) technique has been successfully applied to many site disordered crystals [22]. However, when applying the SQS method to *AgBiI*₄ cells, the crystals generated were metallic [20,23], in contradiction to

E-mail address: brt10@psu.edu (B.R. Tuttle).

 $^{^{\}ast}$ Corresponding author.

experiment. Recent studies found dramatic variations of unit cell energy for $AgBiI_4$ depending on the occupation choices and only low energy cells had reasonable band gaps [20]. For the present investigation, we employ the new spherical cluster method, which has recently been employed to elucidate the atomic structure and properties of several silver iodo-bismuthates, including $AgBiI_4$, Ag_2BiI_5 and Ag_3BiI_6 [20].

Our main result is the determination of energy-structure relationships in $CuBiI_4$ crystal site disordered configurations (Figs. 1, 4 and 5). We find the lowest energy unit cell configuration has bismuth bonding topologies that minimize Bi-Bi interactions (Fig. 6). Accurate band gap calculations show the low energy $CuBiI_4$ cells found have gaps close to the experimental range. Other properties examined include the lattice parameter, density, and the bulk moduli. Importantly, we calculate the Helmholtz free energy and show that configurational entropy leads to the stabilization of the site disordered $CuBiI_4$ crystals. The atomic unit cell models found here will be useful in many $CuBiI_4$ studies, including point defect engineering for improved photovoltaic applications.

2. Models and methods

a) unit cell models

The $CuBiI_4$ crystal primitive cell model considered, shown in Fig. 1, is a site disordered crystal with a cubic space group of $Fd\overline{3}m$ and site occupancy probabilities set to mimic experimentally observed $CuBiI_4$ crystals. Model images were generated with the VESTA computational package [24]. The model in Fig. 1 is based on $CuBiI_4$ crystals with three sub-lattices as determined from early X-ray diffraction experiments [19]. One sub-lattice has 32 fixed iodine atoms as indicated by the small purple balls in Fig. 1. Another sub-lattice has 16 sites represented by large pink-white spheres in Fig. 1; these 16 sites are shared between bismuth and vacancies with equal probabilities. The third sub-lattice involves 64 sites shared between copper and vacancies with copper occupying the sites with 1/8 or 12.5 % probability resulting in 8 copper atoms in the unit cell. Due to site disorder, there are over 10^{13} possible unit cell configurations to consider. The copper site occupation probabilities found by Fourcroy [19] are slightly more complicated than

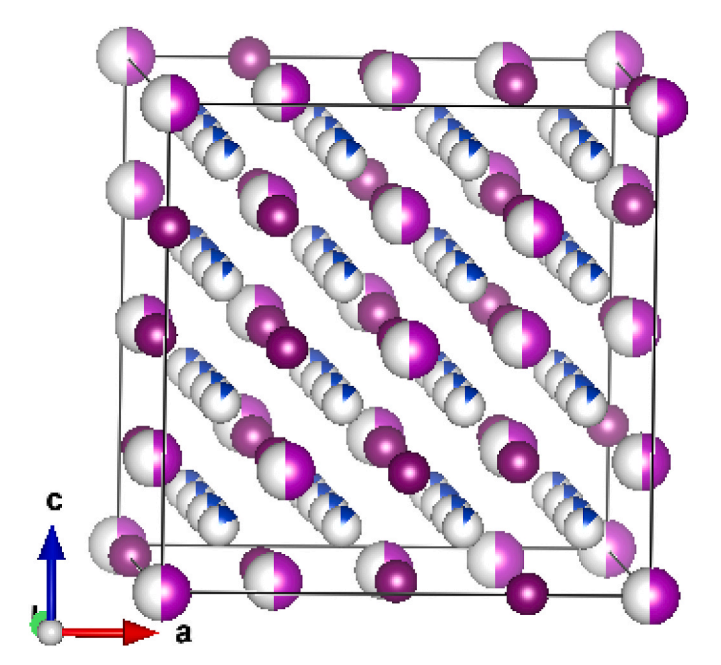


Figure 1. Atomic model of the site disordered crystal of I_4 . The small purple spheres represent iodine atoms. For the larger spheres, pink represents bismuth and white represents a vacancy occupation of the site. For the small white-blue spheres are shared between copper and vacancies.

considered here which would require a larger modeling effort including $\sim 10^{100}$ possible atomic combinations, which is beyond the scope of our present computational abilities.

b) electronic structure methods

The Vienna Ab Initio Simulation Package (VASP [43], [44] version 6.4.1) is used for all density functional theory (DFT) calculations [25, 26]. We employ standard PAW potentials to represent the core-electrons. [45], [46] Specifically, the valence electrons included are $(4s^1\ 3\ d^{10})$ for copper, $(6s^2\ 6p^3)$ for bismuth and $(5s^2\ 5p^5)$ for iodine. For the plane-wave basis function expansion, the cutoff energy of E_c = 250 eV is used for the total energy calculations used to fit the cluster energy model, while $E_c = 400 \, eV$ is used for the final results reported below. For energy calculations, we treat exchange-correlation effects with the PBEsol functional [27,28]. For final reported results, atoms and lattice vectors are allowed to relax until a force tolerance of 0.02 eV/Å is reached. For CuI and Bil₃ crystal energy calculations, we use converged k-point grids for integrations over the Brillouin zone, while for CuBiI4 models, we find a single Γ point calculation is sufficient. Tests indicate our final relative energies are numerically converged to less than 0.001 eV per formula unit. See supplemental section for details on test calculations. Starting from the equilibrium structures at the PBEsol level, we further relax the atomic positions using a method combining the HSE hybrid functional [29,30] and spin-orbit (SO) coupling [31] to determine accurate band gap values. Previously, it has been found that both HSE and SO terms are required for accurate band gaps, due to the large iodine and bismuth atoms [10]. The DFT methods employed here have been validated for electronic and structural properties of similarly complex materials such as $Ag_xBi_yI_{x+3y}$ [10,20], KSrBi [32] and Ba_2NbRhO_6 [33].

c) spherical cluster/simulated annealing-cooling methods

As mentioned in the Introduction, the number of possible atomic arrangements in our site disordered CuBiI₄ unit cell is more than 10¹³, which prevents finding the low energy cells from DFT calculations alone. Instead, we employ the spherical cluster expansion method developed recently by some of the present authors [20]. See Ref. [20] for a longer discussion of the spherical cluster expansion method including a comparison with other competing methods. In the spherical cluster expansion method, each atomic site is assigned an energy based on the location and occupations of other nearby sites. Both atoms and vacancies are considered explicitly. Fitting the cluster model requires calculating the static energy of hundreds of unit cells using DFT, as described above. Once the cluster model is constructed, then we employ an annealing-cooling simulation to search for low energy CuBiI4 unit cells. Simulated annealing in our approach [20] involves starting with a random configuration and then swapping two nearby sites. A swap is always accepted if it lowers the system energy; otherwise, the swap is

accepted at a probability rate (P) set by a Boltzmann factor: P =

 $\exp\left(-\frac{\Delta E}{\tau}\right)$ where ΔE is the change in energy of the system after the swapping of two site occupations and τ is the simulation temperature set in units of energy. The simulation starts at a high simulation temperature such that most swaps are accepted, which simulates system annealing. Then, gradually we lower the temperature to simulate cooling and allow the system to converge on the global minimum energy configurations.

3. Simulation results

In this section we describe the combinatorics, fitting the cluster model, and running the annealing-cooling simulation. In Section IV, we

determine the physical and electronic properties for several $CuBiI_4$ unit cell configurations.

a) combinatorics and symmetry

For site-disordered crystals with two possible site occupations, the number of possible combinations can be calculated with the function $N=\frac{n!}{k!(n-k)!}$ where n is the total number of sites and k is the number of sites occupied by one species. For the bismuth-vacancy sub-lattice in Fig. 1, there are 16 sites and 8 bismuth atoms occupy half the sites so $N=\frac{16!}{8!8!}=12,870$ possibilities. For the copper-vacancy sublattice, we find $N=\frac{64!}{8!56!}\approx 4.426x10^9$ possibilities. Therefore, the total number of combinations is $\approx 5.7x10^{13}$. Using the "disorder" simulation package [34], one can generate the symmetry irreducible site occupancy configurations. We find the sub-lattice with 12,870 possibilities reduces to 97 inequivalent configurations. For each of the unique 97 cases, both the iodine and the bismuth atoms are fixed in their initial sub-lattice sites; only the 8 copper atoms need to be placed among the possible 64 sites.

b) fitting cluster energy model

As noted in Section II, the cluster energy expansion method requires using DFT calculations to determine the energy of each site within the site disordered crystal. For our CuBiI4 crystals, a second nearest neighbor setting with a central site and 12 neighboring sites per cluster can be found by using a spherical cutoff distance of 3.1 Å. Tests found that a first nearest neighbor model is not sufficiently accurate to find the lowest energy configurations. We find 123 unique clusters are sufficient to describe all possible CuBiI4 second neighbor configurations. The site cluster energies are found by fitting to explicit DFT total energy calculations. We use three cells per cluster in our fitting so 369 cells are used. The spherical cluster fitting method is designed to select fitting cells that result in a linearly independent system, so that site cluster energies are well-defined [20]. In order to manage submitting the 369 VASP jobs on a Unix batch system, we use a program called VBHTC [35], which periodically checks to see if any submitted jobs have been completed and automatically submits jobs whenever possible.

For site disordered crystal energies, the present cluster energy (C. E.) model has been shown to perform better than modern machine learning methods that use kernel ridge and decision tree regressions [20]. In addition to the 369 cells that were used to fit the spherical cluster model, we also calculated a test set including 256 models. The results for the predicted energies of the test set agree well with the DFT calculations, as shown in Fig. 2. The blue line shown in Fig. 2 represents perfect agreement. The C. E. model does well at predicting energies for most supercells with a mean absolute error of only $1.2\,\text{meV/atom}$. The C. E. model does particularly well for the very lowest energy cells in the test set, which encourages confidence that our method is accurate enough to find a global minimum out of billions of possibilities.

Section II(c) describes the simulated annealing-cooling approach applied in this study. Fig. 3 shows the energy versus time step for a simulated annealing-cooling of one fixed Bi arrangement but varying the copper site occupations. The spherical cluster energy (C.E.) method's predicted energy per atom is on the vertical axis and simulation step from zero to 10 million is on the horizontal axis. For clarity, not all data points are included in the plot. The black data points are the simulation C. E. energy results, and the red line shows the variation of temperature with simulation step. The blue line shows the energy of the optimal or lowest energy configuration at a given step. As steps increase, the simulation temperature decreases, and the simulation converges to find the globally lowest energy configuration. In the example shown, the simulation finds the minimum energy configuration after less than 2 million steps. We ran the simulation 10 times for each of the 97 symmetrically distinct cases. For all 10 simulation runs, the simulation converges to find the same global minimum energy configuration.

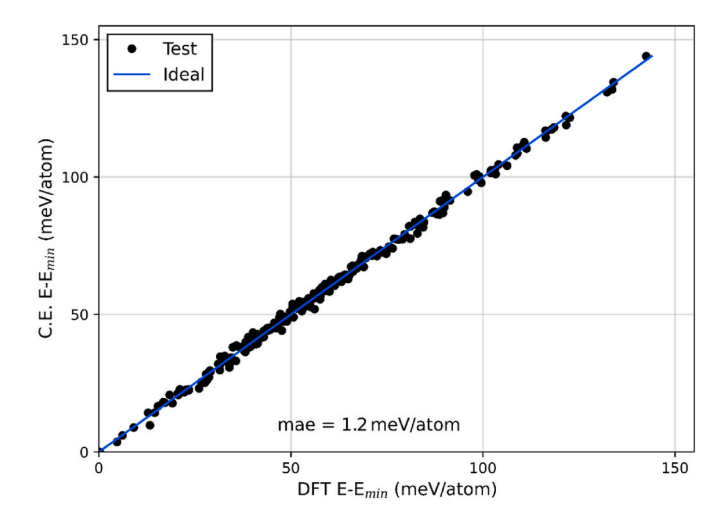


Fig. 2. The average energy per site is reported for test data set using the predicted values from the cluster energy (C. E.) method and the calculated *ab inito* energies (DFT). The mean absolute error is 1.2 meV/atom. The blue perfect fit line is $\gamma=x$.

c) simulated annealing - cooling.

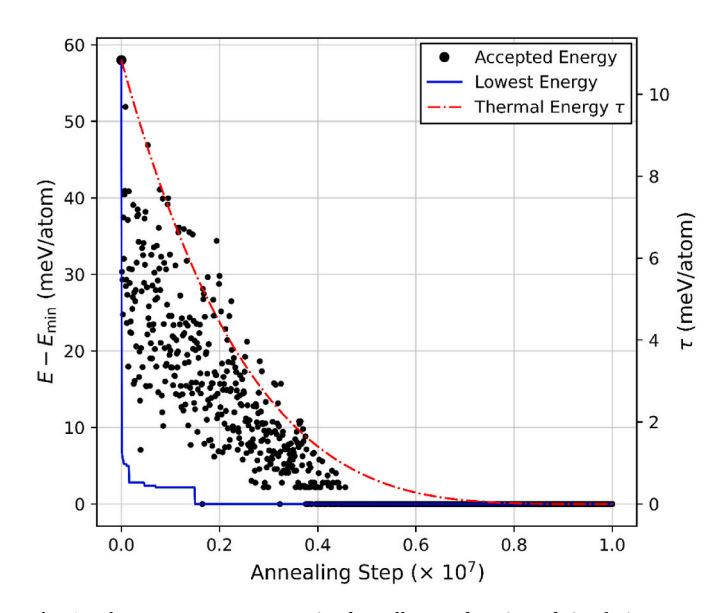


Fig. 3. The average energy per site for cells as a function of simulation step. The energies are from the cluster method and the simulation temperature has units of eV.

The energy for each of the 97 unit cells with unique Bi arrangements are shown in Fig. 4. These energies are found from annealing-cooling simulations as shown in Fig. 3 along with a final DFT energy minimization calculation at fixed volume. Most unit cells are between ≈ 5 and $\approx 20~meV/atom$ higher than the lowest energy unit cell. Only one unit cell is within 1 meV of the lowest energy unit cell. The first and second lowest energy unit cells are labelled Model Bi1 and Bi2, respectively, and these models are subjected to more detailed consideration below.

The atomic arrangements of the two lowest energy cells (See Fig. 4) are shown in Fig. 5. The lowest energy Bi1 model includes linear chains for CuI_4 tetrahedra with neighboring tetrahedra sharing two iodine atoms. For all Cu atoms, there are two CuI bonds with lengths 2.58 Å and two bonds with lengths 2.71 Å. The second lowest energy Bi2 model includes two clusters of CuI tetrahedra, where the CuI bonds have variable lengths from 2.50 Å and 2.65 Å. For the Bi1 model, the BiI bonds have lengths of 3.07 Å in four cases and 3.12 Å in two cases. The BiI

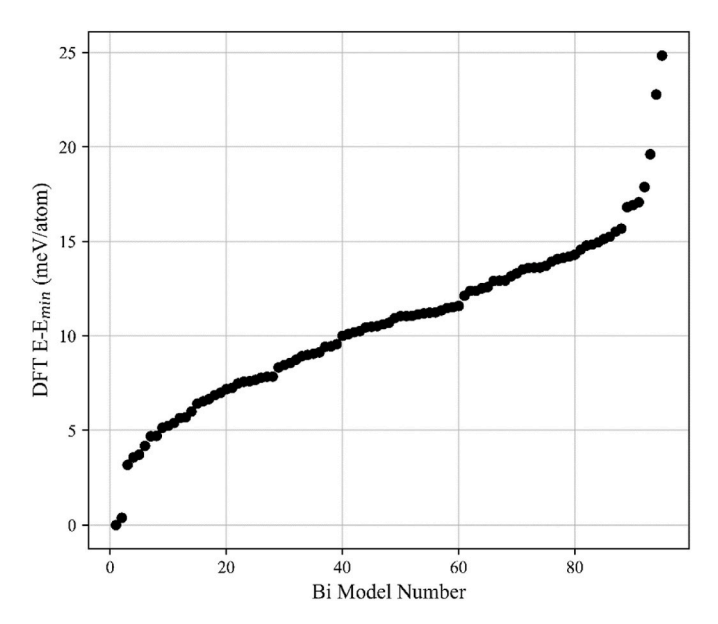


Fig. 4. The average energy per site for the minimum energy cells displayed from lowest to highest energy for each of the 97 symmetrically unique Bi configurations. The energies are from the cluster method and are in units of eV/site.

bonds for the Bi2 models have variable lengths from 3.01 Å and 3.25 Å. In all cases the I, Bi, I bond angle is \approx 90 degrees.

The ordering of bismuth in these models shows interesting patterns. Fig. 6 was generated by removing the Cu and I atoms from Fig. 5 and adding bond connections between the Bi atoms that are within 4.4 Å. Finally, periodic image Bi atoms are added to better show the topology of the Bi chains. The lowest energy Bi1 model has two zig-zag chains of bismuth [BiI6 octahedra] oriented along one axis (see Fig. 6 left). The bismuth atoms are expected to only weakly interact with each other since they are $\approx 4.3 \, \text{Å}$ apart and are bound to the closer iodine atoms. The topological arrangements of Bi atoms found here are also found in AgBiI₄ cells [10]. As discussed previously [10], the Bi arrangements shown in Figs. 5 and 6 allow the Bi atoms to distribute more evenly throughout the unit cell thereby minimizing the number of nearby Bi-Bi pairs. Because of the ionic nature of Bi atoms in CuBiI4, fewer Bi-Bi interactions facilitates lower energy unit cells. Higher energy cells involving more Bi-Bi interactions also results in significantly lower band gaps indicating a reduction in the overall covalency in these configurations.

4. Analysis

We consider two models for further analysis whereby we fully relax the atoms and volumes using the methods discussed in Section II(b). The two models (Bi1 and Bi2) are from our C.E. simulated annealing-cooling results discussed above.

In Table 1, we present our calculations for the lattice constant (a), mass density (ρ) , and band gap (E_g) for the $CuBiI_4$ unit cell models

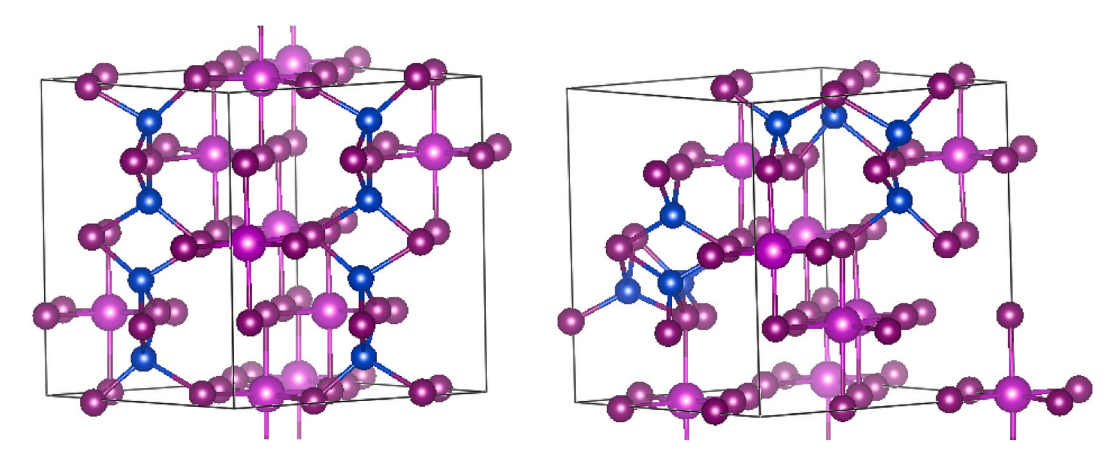


Fig. 5. Ball and stick models for Bi1 (left) and Bi2 (right) CuBiI4 models discussed above.

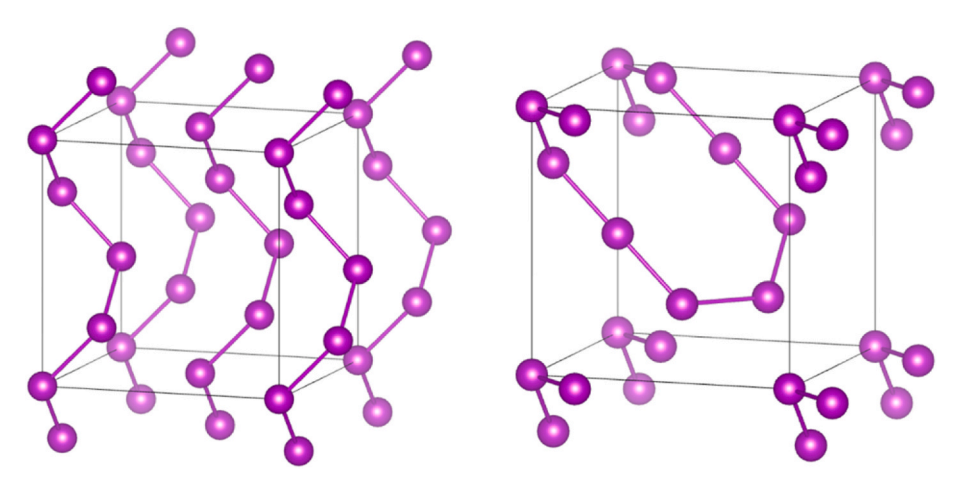


Fig. 6. The ball-and-stick image of only the Bi atoms in the lowest (left) and second lowest (right) energy CuBiI₄ cells found as reported in Figs. 4 and 5.

Table 1

The present results are compared with the experimental values of the lattice constant (a), the density (ρ) , and the direct band gap (E_g) . The Also included are the theoretical values for the bulk modulus (B) and the change in free energy (ΔF) . See text for a description of thermodynamic average results reported in the last row.

	a (Å)	$\rho \left(g/cm^{3} \right)$	B(GPa)	$\Delta F\left(eV\right)$	$E_g(eV)$
Experimental	12.13	5.82	_	_	1.79 [11] -
	[19]				1.84 [16]
Model Bi1	12.20	5.72	10.4	+0.09	1.84
Model Bi2	12.17	5.76	14.4	+0.16	1.80
Ave (T = 600K)	12.185	5.74	12.4	- 0.07	1.82

discovered in this study along with experimental values. The lattice constant and bulk modulus is found by fitting the energy versus volume to a fourth order polynomial using five data points with \pm 6 % of the minimum-energy volume. In addition, we calculate the change in the Helmholtz free energy per formula unit (ΔF) by comparing $CuBiI_4$ to its precursor components CuI and I_3 :

 $\Delta F = E(CuBiI_4) - E(CuI) - E(BiI_3) - S_{conf}T$. Here we ignore vibrational entropic effects which are expected to be small because the bonding environments in $CuBiI_4$ are similar to those in BiI_3 and CuI. For instance, in $CuBiI_4$ there are four Cu-I bonds with lengths ≈ 1.6 Å as is found in CuI. The vibrational entropic contributions mainly cancel, as has been found in a recent analysis of high entropy MoNbTaW [36], with the overall effect on ΔF estimated to be less than 0.01 eV per formula unit. A positive value of ΔF means the $CuBiI_4$ phase separates into the two binary alloys. While a complete analysis of the Cu-Bi-I phase diagram is beyond the scope of the present study, we do determine the configurational entropy (S_{conf}) for $CuBiI_4$ using standard methods [37]. Considering the degeneracy of the Bi1 and Bi2 models, we calculate the thermodynamic average properties for $CuBiI_4$ and report these in Table 1.

The *CuBiI*₄ models have lattice constants 12.20 Å (Model Bi1) and 12.17 Å (Model Bi2). Both values are slightly larger than experiment. This is reasonable since the PBEsol method used to calculate the lattice constants tends to overestimate lattice constants and underestimate density. Models Bi1 and Bi2 have similar densities close to experiment which is expected given the good lattice constant values. The bulk moduli found here are $\sim 10~GPa$, close to a value calculated previously in Ref. [11]; these moduli are much softer than typical photovoltaic materials (e.g. Si and CdTe), by a factor of 10 or more, but are only slightly larger than the established value for BiI_3 .

Photoluminescence experiments indicate \textit{CuBil}_4 is a direct gap semiconductor, which is because the configurational site disorder breaks long range symmetries. Therefore, we only report the direct band gap at Γ for the Bi1 and Bi2 models in Table 1, along with the \textit{CuBil}_4 direct band gap found from photo-luminescence experiments. The calculated band gap of our models (Bi1 and Bi2) are within the experimental range. Not shown in Table 1 are the band gap results at the PBE and HSE levels which are $\approx 1.5~eV$ and $\approx 2.6~eV$, respectively. This confirms previous work [10] that shows the importance of including hybrid functionals and spin-orbit coupling in the calculation of band gaps for heavy metal halide semiconductors.

The cubic phase $CuBiI_4$ models found here have a positive ΔF when ignoring configurational site disorder. However, because of site-disorder in $CuBiI_4$ crystals, entropy may stabilize the cubic phase. Using standard thermodynamic averaging [37], we calculate the average properties for $CuBiI_4$ using our Bi1 and Bi2 models assuming such a two state system can represent the whole $CuBiI_4$ crystal. Because these models are the lowest in energy, they will be most important in determining the overall crystal properties. Most $CuBiI_4$ crystals are grown using solution-based methods [6] at $T\approx 600K$, which is the temperature we use to calculate thermodynamic average properties. The entropic term is confined to

configurational entropy. The number of equivalent configurations (i.e. the degeneracy) for the Bi1 and Bi2 models is 12 and 48, respectively. At T=600K, we find the Bi1 and Bi2 models coincidentally have almost equal contributions (49 % and 51 %, respectively) to the thermodynamic average, so the mechanical and electronic properties are simply the average of the Bi1 and Bi2 results. Using the Helmholtz free energy expression above, we determine that $\Delta F=-0.07~eV$ for the $CuBiI_4$ system including entropy of mixing the Bi1 and Bi2 models. This negative ΔF result indicates that $CuBiI_4$ is thermodynamically stable due to entropic effects.

The ΔF value depends critically upon the energy of the $CuBiI_4$ model considered. As noted in the Sect. II(a), the models considered here are limited to 8 CuBiI₄ formula units per cell. Employing larger supercell models, would allow for more strain relief and for the copper occupancy to be closer to the experimental values. To estimate the strain relief term. we construct a $2 \times 2 \times 2$ supercell of the Bi1 model and relax its coordinates. We find that strain relief lowers the Bi1 supercell energy by 0.006 eV per formula unit. As illustrated in Fig. 3, the energy of CuBiI₄ is sensitive to the occupation sites of the copper atoms. The energy reduction from the more accurate copper occupations in a larger CuBiI₄ model can be estimated from the energy variations found in Fig. 3. Specifically, the energy difference between the lowest Bi1 energy model and the next lowest energy copper occupancy model is 2 meV per atom or 0.012 eV per formula unit. Adding these two effects, we estimate the smaller models used in this study result in ΔF values $\approx 0.02 \, eV$ per formula unit too high.

To investigate the relationship between electronic structure and atomic structure, we examine the chemical nature of the band edge states for the Bi1 and Bi2 models, as shown in Fig. 7 and in supplemental section. Fig. 7 shows the density of states as a function of state energy with the Fermi energy at 0.0 eV. The Bi1 model includes two sets of linear chains each with four CuI tetrahedra while the Bi2 model includes two isolated clusters of four CuI tetrahedra. See supplemental section for iso-surface plots for the band edge states. In both Bi1 and Bi2 models, the valence band edge states involve non-bonded iodine p-orbitals whereas the conduction band edge states are mainly localized on the bismuth and

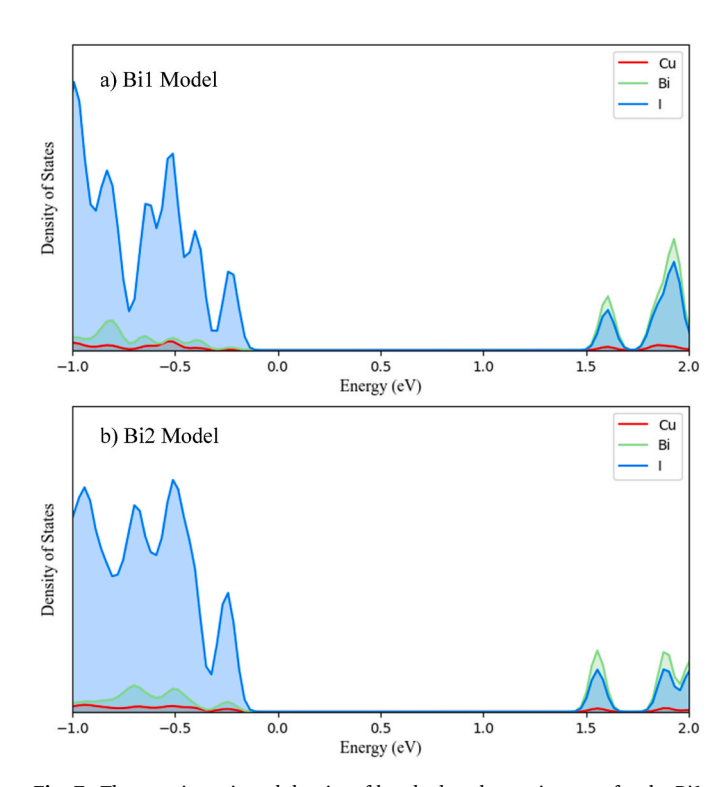


Fig. 7. The atomic projected density of band edge electronic states for the Bi1 and Bi2 models.

iodine atoms. Despite the differing arrangement of bismuth and copper atoms, the band edge states in the Bi1 and Bi2 models are very similar in character.

5. Discussion and conclusions

Density functional energy calculations are fitted to a spherical cluster-expansion empirical model which is used in an annealing-cooling simulation to search $\approx 10^{13}$ atomic configurations for physically relevant atomic configurations for $CuBiI_4$ unit cells. We also identify Bi chains that correlate with low energy configurations. The lattice constant and band gap of the newly discovered lowest energy unit cells compare favorably to the respective experimental results. We also find spin-orbit coupling is critical for accurate band gap results for $CuBiI_4$ and should be used in similar heavy metal halide systems. Finally, we predict that $CuBiI_4$ has a bulk modulus closer to BiI_3 similar to previous calculations.

Entropy stabilized crystals are an important class of materials with interesting and unique properties. High entropy metal alloys have long been recognized for having high strength and excellent corrosion resistance. More recently multi-component entropy stabilized oxides show significant promise for engineering by cation composition [38]. While cubic $CuBil_4$ has been studied for many decades [19], this appears to be the first recognition that it is an entropy stabilized semiconductor alloy. The analysis here suggests a large number of ternary metal halides may also be entropy stabilized with numerous opportunities for growing quaternary mixes with unique properties, as has been recently investigated [6].

The $CuBiI_4$ models reported here can be used to develop an atomic level understanding of devices based on $CuBiI_4$ semiconductors. For instance, with some effort one can calculate effective electron and hole masses, as has been done recently for $AgBiI_4$ [10,20]. These effective masses are needed in simulations of photovoltaic and other devices. Defect engineering is another area of interest. Atomic calculations have recently elucidated the role of defects in ternary metal halides including $AgBiI_4$ [39] and $Rb_3Sb_2I_9$ [40]. For $Rb_3Sb_2I_9$ solar cells, recently observed current limiting defects [41] have been identified [40] from atomic calculations. Also, $CuBiI_4$ heterojunctions employed in photovoltaics and other applications can be examined starting from the present atomic models. Overall, the present $CuBiI_4$ models can be used to improve our understanding of $CuBiI_4$ in various device applications.

The atomic models identified herein agree with experimental measures and present a proper starting point for the study of atomic-level structure-property relations in $CuBiI_4$ devices. The present approach and findings provide a platform for future studies of the structural and electronic properties of $CuBiI_4$ and related site disordered metal-halide semiconductors.

CRediT authorship contribution statement

Blair R. Tuttle: Writing – review & editing, Writing – original draft, Visualization, Validation, Supervision, Software, Resources, Project administration, Methodology, Investigation, Funding acquisition, Formal analysis, Data curation, Conceptualization. John R. Bickel: Investigation. Zach J. Willard: Investigation. Victor T. Barone: Formal analysis. Sanjay V. Khare: Formal analysis.

Novelty statement

The importance of atomic ordering in high entropy systems has been a long standing materials problem. CuBiI4 is a system where several atoms and vacancies share crystalline sites, so-called atomic site-occupancy disorder. A highlight of the present research is the fitting of a new cluster-energy (CE) model using high-throughput DFT calculations; with this CE model, we sort through 10¹³ possible atomic configurations using Monte Carlo to identify the physically important ones.

Another highlight of this research is that it is the first to provide evidence of entropy stabilization of the cubic phase. The importance of entropy identified along with the atomic models discovered allows for the investigation of doping CuBil4 in order to design unique semiconductors, similar to the design of super-hard high entropy metals. Finally, the new atomic models will be important for an atomic level investigation of CuBil4 in device applications; for instance, the models discovered can be used in effective mass and band offset calculations as well as defect engineering analysis. Sincerely, Blair Tuttle, Professor of Physics, Penn State BehrendData available upon reasonable request.

Declaration of competing interest

The authors declare the following financial interests/personal relationships which may be considered as potential competing interests: Blair Tuttle reports financial support was provided by National Science Foundation. If there are other authors, they declare that they have no known competing financial interests or personal relationships that could have appeared to influence the work reported in this paper.

VI. Acknowledgements

BRT would like to acknowledge support from National Science Foundation under grant DMR-2127473. Computations for this research were performed on the Pennsylvania State University's Institute for Computational and Data Sciences' Roar supercomputer.

Appendix A. Supplementary data

Supplementary data to this article can be found online at https://doi.org/10.1016/j.physb.2025.417888.

Data availability

Data will be made available on request.

References

- [1] A.K. Jena, A. Kulkarni, T. Miyasaka, Halide perovskite photovoltaics: background, status, and future prospects, Chem. Rev. 119 (5) (2019/03/13 2019) 3036–3103.
- [2] D.H. Fabini, et al., Main-group halide semiconductors derived from perovskite: distinguishing chemical, structural, and electronic aspects, Inorg. Chem. 56 (1) (2017/01/03 2017) 11–25.
- [3] J.-C. Hebig, I. Kühn, J. Flohre, T. Kirchartz, Optoelectronic properties of (CH3NH3) 3Sb2I9 thin films for photovoltaic applications, ACS Energy Lett. 1 (1) (2016/07/ 08 2016) 309–314.
- [4] S. Sun, S. Tominaka, J.-H. Lee, F. Xie, P.D. Bristowe, A.K. Cheetham, Synthesis, crystal structure, and properties of a perovskite-related bismuth phase, (NH4) 3Bi2I9, APL Mater. 4 (3) (2016) 031101.
- [5] G. Kakavelakis, M. Gedda, A. Panagiotopoulos, E. Kymakis, T.D. Anthopoulos, K. Petridis, Metal halide perovskites for high-energy radiation detection, Adv. Sci. 7 (22) (2020) 2002098.
- [6] A. Chakraborty, N. Pai, J. Zhao, B.R. Tuttle, A.N. Simonov, V. Pecunia, Rudorffites and beyond: perovskitte-inspired silver/copper pnictohalides for next-generation environmentally friendly photovoltaics and optoelectronics, Adv. Funct. Mater. 32 (36) (2022) 2203300.
- [7] L.F. Mashadieva, Z.S. Aliev, A.V. Shevelkov, M.B. Babanly, Experimental investigation of the Ag-Bi-I ternary system and thermodynamic properties of the ternary phases, J. Alloys Compd. 551 (2013/02/25/2013) 512–520.
- [8] I. Turkevych, et al., Photovoltaic rudorffites: lead-free silver bismuth halides alternative to hybrid lead halide perovskites, ChemSusChem 10 (19) (2017) 3754–3759.
- [9] N. Pai, et al., Silver bismuth sulfoiodide solar cells: tuning optoelectronic properties by sulfide modification for enhanced photovoltaic performance, Adv. Energy Mater. 9 (5) (2019) 1803396.
- [10] V.T. Barone, B.R. Tuttle, S.V. Khare, Properties of AgBil4 using high through-put DFT and machine learning methods, J. Appl. Phys. 131 (24) (2022).
- [11] A. Das, K. Pal, P. Acharyya, S. Das, K. Maji, K. Biswas, Strong antibonding I (p)—Cu (d) states lead to intrinsically low thermal conductivity in CuBiI4, J. Am. Chem. Soc. 145 (2) (2023/01/18 2023) 1349–1358.
- [12] V. Pecunia, et al., Roadmap on energy harvesting materials, J. Phys.: Materials 6 (4) (2023/08/07 2023) 042501.

- [13] C. Polyzoidis, K. Rogdakis, E. Kymakis, Indoor perovskite photovoltaics for the Internet of things—challenges and opportunities toward market uptake, Adv. Energy Mater. 11 (38) (2021) 2101854.
- [14] H. Yu, et al., Gradient formation and charge carrier dynamics of CuBiI4 based perovskite-like solar cells, Sustain. Energy Fuels 4 (6) (2020) 2800–2807, https://doi.org/10.1039/C9SE01288E.
- [15] B. Zhang, et al., An in-situ room temperature route to CuBiI4 based bulkheterojunction perovskite-like solar cells, Sci. China Mater. 62 (4) (2018) 519–526.
- [16] N. Qu, et al., From Bil3 to CuBil4: a striking improvement in the photoelectric performance of a novel photodetector candidate, J. Mater. Chem. C 8 (25) (2020) 8451–8456, https://doi.org/10.1039/D0TC01188F.
- [17] Z. Hu, et al., Solution-processed air-stable copper bismuth iodide for photovoltaics, ChemSusChem 11 (17) (2018) 2930–2935.
- [18] L. Wang, et al., Revealing the potential crystal structures of earth-abundant nontoxic photovoltaic CuBil4, Cryst. Growth Des. 21 (5) (2021/05/05 2021) 2850–2855.
- [19] P.H. Fourcroy, D. Carré, F. Thévet, J. Rivet, Structure du tétraiodure de cuivre(I) et de bismuth(III), CuBiI4, Acta Crystallogr. C 47 (10) (1991) 2023–2025.
- [20] V.T. Barone, B.R. Tuttle, S.V. Khare, Spherical cluster method for ground state determination of site-disordered materials: application to Ebebiyin+3y, Comput. Mater. Sci. 231 (2024) 112587, 2024/01/05/.
- [21] L. Bellaiche, D. Vanderbilt, Virtual crystal approximation revisited: application to dielectric and piezoelectric properties of perovskites, Phys. Rev. B 61 (12) (2000) 7877–7882.
- [22] A. Zunger, S.H. Wei, L.G. Ferreira, J.E. Bernard, Special quasirandom structures, Phys. Rev. Lett. 65 (3) (1990) 353–356.
- [23] B. Cucco, L. Pedesseau, C. Katan, J. Even, M. Kepenekian, G. Volonakis, Silver–bismuth halide double salts for lead-free photovoltaics: insights from symmetry-based modeling, Sol. RRL 6 (12) (2022) 2200718.
- [24] K. Momma, F. Izumi, VESTA 3 for three-dimensional visualization of crystal, volumetric and morphology data, J. Appl. Crystallogr. 44 (6) (2011) 1272–1276.
- [25] P. Hohenberg, W. Kohn, Inhomogeneous electron gas, Phys. Rev. 136 (3B) (1964) B864–B871.
- [26] W. Kohn, L.J. Sham, Self-consistent equations including exchange and correlation effects, Phys. Rev. 140 (4A) (1965) A1133–A1138.
- [27] J.P. Perdew, K. Burke, M. Ernzerhof, Generalized gradient approximation made simple, Phys. Rev. Lett. 77 (18) (1996) 3865–3868.

- [28] J.P. Perdew, et al., Restoring the density-gradient expansion for exchange in solids and surfaces, Phys. Rev. Lett. 100 (13) (2008) 136406.
- [29] J. Heyd, G.E. Scuseria, M. Ernzerhof, Hybrid functionals based on a screened Coulomb potential, J. Chem. Phys. 118 (18) (2003) 8207–8215.
- [30] J. Heyd, G.E. Scuseria, M. Ernzerhof, "Erratum: "Hybrid functionals based on a screened Coulomb potential" [J. Chem. Phys. 118, 8207 (2003)],", J. Chem. Phys. 124 (21) (2006) 219906.
- [31] S. Steiner, S. Khmelevskyi, M. Marsmann, G. Kresse, Calculation of the magnetic anisotropy with projected-augmented-wave methodology and the case study of disordered \${\mathrm{Fe}}_{1\end{e}}_{1\end{e}} \nusure \text{mathrm{Co}}_{x} \text{alloys, Phys. Rev. B 93 (22) (2016) 224425, 06/23/.
- [32] D. Behera, et al., First principles studies on optoelectronics and transport properties of KSrY (Y = Sb, Bi) for renewable energy application, Mater. Sci. Eng., B 297 (2023/11/01/2023) 116765.
- [33] S. Belhachi, et al., DFT analysis of Ba2NbRhO6: a promising double perovskite for sustainable energy applications, J. Inorg. Organomet. Polym. Mater. 35 (2) (2025/ 02/01 2025) 978–993.
- [34] J.-C. Lian, H.-Y. Wu, W.-Q. Huang, W. Hu, G.-F. Huang, Algorithm for generating irreducible site-occupancy configurations, Phys. Rev. B 102 (13) (2020) 134209, 10 (22)
- [35] V.T. Barone, Vbhtc [Online]. Available: https://github.com/victorbarone5066.
- [36] Y. Huang, M. Widom, Vibrational entropy of crystalline solids from covariance of atomic displacements, Entropy 24 (5) (Apr 28 2022) (in eng).
- [37] R. Grau-Crespo, S. Hamad, C.R.A. Catlow, N.H. de Leeuw, Symmetry-adapted configurational modelling of fractional site occupancy in solids, J. Phys. Condens. Matter 19 (25) (2007/05/31 2007) 256201.
- [38] C.M. Rost, et al., Entropy-stabilized oxides, Nat. Commun. 6 (1) (2015/09/29 2015) 8485.
- [39] Q. Yan, et al., Theoretical defect engineering in AgBiI4 for enhanced photovoltaic performance, Appl. Phys. Lett. 127 (4) (2025).
- [40] B.R. Tuttle, E.J. Payne, Z.J. Willard, S.V. Khare, V. Pecunia, Atomic theory of point defect assisted carrier recombination in Rb3Sb2I9, J. Phys. Chem. Solid. 208 (2026/01/01/2026) 113190.
- [41] V. Pecunia, et al., Photoinduced current transient spectroscopy: assessing the impact of defects on lead-free perovskite-inspired photovoltaics via photoinduced current transient spectroscopy (Adv. Energy mater. 22/2021), Advanced Energy Materials 11 (22) (2021) 2170082.